Jovian auroral radio source occultation modelling and application to the JUICE science mission planning

Baptiste Cecconi, Corentin K. Louis, Claudio Muñoz Crego, Claire Vallat

Planetary and Space Science 209 (2021) 105344

Contents lists available at ScienceDirect

Planetary and Space Science

journal homepage: www.elsevier.com/locate/pss

Jovian auroral radio source occultation modelling and application to the JUICE science mission planning

Baptiste Cecconi [a,*], Corentin K. Louis [b], Claudio Muñoz Crego [c], Claire Vallat [d]

[a] LESIA, Observatoire de Paris, CNRS, PSL Research University, Meudon, France
[b] School of Cosmic Physics, DIAS Dunsink Observatory, Dublin Institute for Advanced Studies, Dublin, Ireland
[c] Aurora B.V., for European Space Agency, ESAC, Madrid, Spain
[d] Rhea Group, for European Space Agency, ESAC, Madrid, Spain

ARTICLE INFO

Keywords:
Planetary radio emissions
Jupiter

ABSTRACT

Occultations of the Jovian low frequency radio emissions by the Galilean moons have been observed by the PWS (Plasma Wave Science) instrument of the Galileo spacecraft. We show that the ExPRES (Exoplanetary and Planetary Radio Emission Simulator) code accurately models the temporal occurrence of the occultations in the whole spectral range observed by Galileo/PWS. This validates of the ExPRES code. In addition to supporting the analysis of the science observations, the method can be applied for preparing the JUICE moon flyby science operation planning.

1. Introduction

The magnetosphere of Jupiter produces low frequency radio emissions near the planetary polar regions, along the active magnetic field lines connected to the Jovian auroral oval as well as to the Galilean moon auroral magnetic footprints. The Jovian radio emissions are intense and non-thermal radio frequency phenomena, spanning from a few kHz to about 40 MHz. They are produced through the Cyclotron Maser Instability (CMI), which converts the local plasma free-energy into electromagnetic radiation (Zarka, 2004; Louarn et al., 2017, 2018). They are used as a proxy for the Jovian magnetospheric activity. They were discovered by Burke and Franklin (1955) and have been since studied with ground observatories (e.g., Nançay Decametre Array, Lamy et al., 2017) and space-borne instruments (with, e.g., the Voyager, Galileo, Cassini and Juno space missions).

Observations from the Cassini Radio and Plasma Wave Science (RPWS, Gurnett et al., 2004) and Galileo Plasma Wave Science (PWS, Gurnett et al., 1992) experiments showed that the Jovian radio emission events are observed quasi-permanently along the spacecraft orbit. Fig. 1 shows 24 h of simultaneously observed spectral flux densities by the Cassini/RPWS and Galileo/PWS instruments, when Cassini was close to its flyby of Jupiter. Both panels of this figure display many arc-shaped radio events (a few of them are highlighted with a thin plain black line), with a few small time-frequency regions with quiet (background level) conditions. Radio arcs can be classified with orientation of their curvature: "vertex-early" and "vertex-late" arcs corresponds to opening "(" or closing ")" parenthesis shapes. The arc shape of Jovian radio emission is well explained by the CMI mechanism at the radio source, coupled with the shape of the magnetic field lines, and the rotation of Jupiter with respect of the observer, as described in Fig. 1 of Louis et al. (2019a). This figure also introduces two other features of the observed radio spectrum around Jupiter: Type III Solar radio bursts are also observed depending on the solar activity (three events are highlighted with a thin dashed black line); and the so-called "attenuation lanes" (Gurnett et al., 1998) resulting from the propagation of hectometric waves through the Io plasma torus (Menietti et al., 2003). The attenuation lanes are observed as a narrow-band attenuation feature modulated at the planetary rotation period. The attenuation is also accompanied or replaced with an intensification of the signal, similar to caustic optical phenomena. The Solar Type III bursts are the only features observed simultaneously on each panel. This illustrates the strong anisotropy of the radio emission features at Jupiter, since the two spacecraft are located at different longitude around the planet.

Although not covering the full spectral range of the Jovian radio emissions, Galileo/PWS routinely collected radio observations during its many orbits in the Jovian system. This data (Gurnett et al., 1997) shows quasi continuous emission from a few 100 kHz up to 5.6 MHz, the upper spectral limit of PWS. During the Galilean moon flybys, Galileo/PWS

* Corresponding author.
E-mail addresses: baptiste.cecconi@observatoiredeparis.psl.eu, baptiste.cecconi@obspm.fr (B. Cecconi), corentin.louis@dias.ie (C.K. Louis), cmunoz@sciops.esa.int (C. Muñoz Crego), cvallat@sciops.esa.int (C. Vallat).

https://doi.org/10.1016/j.pss.2021.105344
Received 12 March 2021; Received in revised form 25 August 2021; Accepted 14 September 2021
Available online 6 October 2021

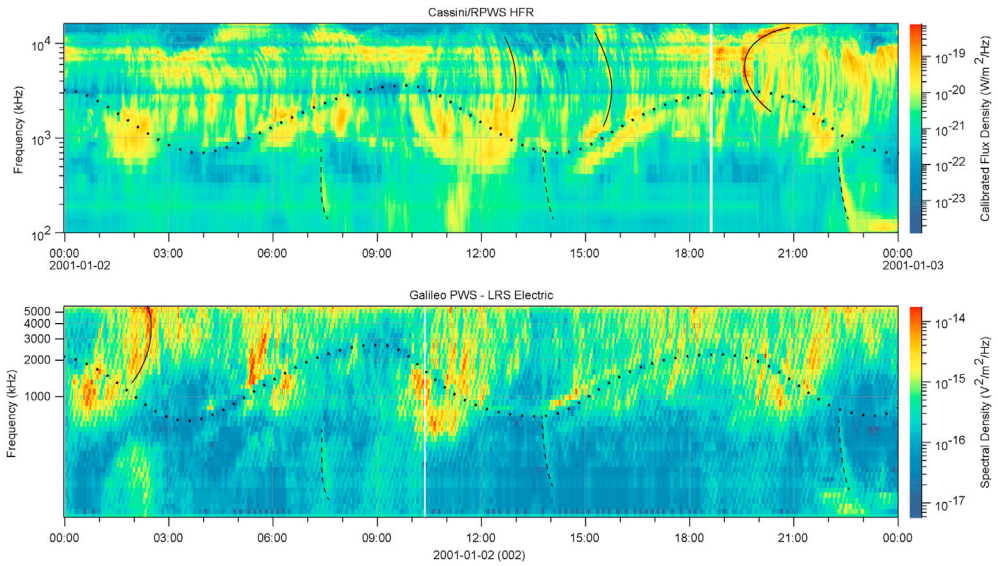

Fig. 1. Calibrated Cassini/RPWS/HFR (Zarka et al., 2004; Cecconi and Zarka, 2019) (top) and GLL/PWS (see Section 2.1) (bottom) radio electric power spectral densities during 24 h close to the Cassini flyby of Jupiter. Significant features have been highlighted: a few radio emission "arcs" are traced in plain line; Type III Solar radio bursts are traced in dashed line; and the attenuation lanes are traced in dotted line.

observed full occultations of the Jovian radio emissions (Kurth et al., 1997).

The ESA JUICE (JUpiter ICy moon Explorer, Witasse, 2019) will explore the Jupiter system and its magnetosphere. The study of the Jovian magnetosphere can strongly benefit from remote observations and modelling tools (Cecconi, 2019). Two instruments of the JUICE scientific payload will operate in the low frequency radio range (below 50 MHz): the Radio and Plasma Waves Instrument (RPWI, Wahlund, 2013) has a receiver dedicated to the study of Jovian radio emissions; and the Radar for Icy Moon Exploration (RIME) experiment (Bruzzone et al., 2013) will operate with a central frequency at 9 MHz, which lies within the Jovian radio emission spectral range. The Jovian radio emission may interfere with RIME active radar mode (Cecconi et al., 2012), but can be also used in a passive radar experiment mode during icy moon flybys (Romero-Wolf et al., 2015; Schroeder et al., 2016; Kumamoto et al., 2017).

The ExPRES code (Exoplanetary and Planetary Radio Emissions Simulator, Louis et al., 2019a) simulates for a given observer the geometrical visibility of radio emissions of a magnetised body. This visibility depends in particular of the angle between the magnetic field vector at the source and the emitted wave vector, which is computed self-consistently in the frame of the CMI theory. The anisotropic shape of the radio source and their geometrical observability conditions are well described in Fig. 1 (panels c, d and e) of Louis et al. (2019a). This computation is iterated at each time/frequency step and for each source. The produced time-frequency map (or dynamic spectrum) can then directly be compared to observations. ExPRES thus provides a characterization (time, frequency, location, polarization, etc.) of the observable auroral radio sources of Jupiter for an observer at a given location. It can be used by any team or processing requiring such kind of information.

In this study, we model the Jovian radio emission occultations during (past) Galileo and (planned) JUICE Galilean moon flybys, using the ExPRES code. We use the ExPRES model results to interpret the Galileo/PWS observed occultations, and show how this model can be used to prepare the JUICE mission science operation planning. We also discuss how the low frequency radio occultation can be used to characterise the Galilean moon's environment.

2. Data sets

Several sets of data have been used in this study and are presented in this section. For the Galileo spacecraft flybys, we compare the actual observed radio spectra with low frequency radio occultations predicted by the ExPRES code, using the actual flyby geometry (spacecraft and moon trajectory in a Jovian reference frame). The JUICE spacecraft study only includes modelled occultations.

2.1. Galileo PWS observations

All Galilean moon flyby of Galileo with PWS data have been modelled and analysed. The Galileo PWS (hereafter referred to as GLL/PWS) data have been retrieved from the University of Iowa *das2* server interface (Piker et al., 2019), using the das2py[1] python module. We have used the *GLL/PWS LRS 152-channel calibrated electric* collection[2] from that *das2* server. The data are radio-electric power spectral densities provided in units of $V^2/m^2/Hz$. This dataset doesn't include the instrument's antenna gain calibration, but this has no consequence on this study. The data set has a native time resolution of 18.67 s. These data are also available in the full resolution GLL/PWS dataset (GO-J-PWS-2-REDR-LPW-SA--FULL-V1.0, Gurnett et al., 1997), at NASA PDS (Planetary Data System) PPI (Planetary Plasma Interaction) node.

2.2. Moons and spacecraft trajectory data

The moons and spacecraft trajectory data are computed using SPICE kernels (Acton, 1996). In this study, the ephemeris data have been retrieved using the NASA-JPL (Jet Propulsion Laboratory of the National Aeronautics and Space Administration) instance of WebGeoCalc (Acton et al., 2018) for the Galileo spacecraft and Jovian moons, and another WebGeoCalc instance at ESA-ESAC (European Space Astronomy Centre of the European Space Agency) for the JUICE spacecraft. The JUICE spacecraft SPICE kernels (ESA SPICE Service, 2020) contains all the studied orbital scenarii, as described in the JUICE CReMA (Consolidated Report on Mission Analysis) documents. In this study, the selected JUICE

[1] Available from https://github.com/das-developers/das2py (last access: 17-Aug-2021).

[2] URI: http://das2.org/browse?resolve=tag:das2.org,2012:site:/uiowa/galileo/pws/survey_electric.

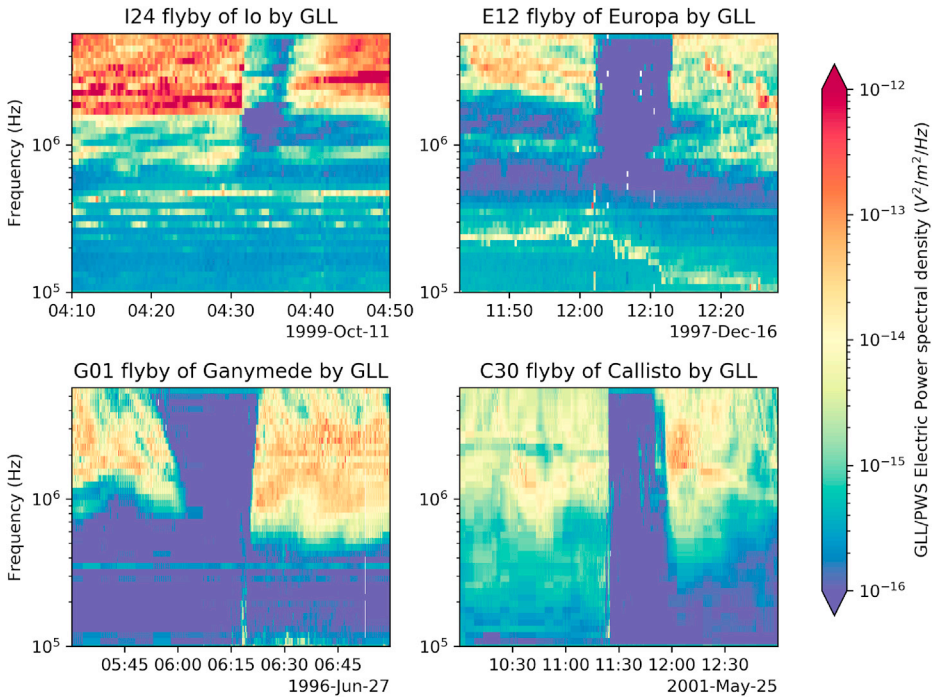

Fig. 2. Jovian radio emission occultations by Io (upper left), Europa (upper right), Ganymede (lower left) and Callisto (lower right), as seen by GLL/PWS. The figures are showing radio electric power spectral densities in $V^2/m^2/Hz$.

trajectory scenario is CReMA version 3.0 (hereafter referred to as CReMA-3.0).[3] The ephemeris of all bodies have been retrieved in the *IAU_JUPITER* reference frame, also referred to as "IAU Jupiter System III (1965)". In the WebGeoCalc interface, we use the "planetocentric" representation for coordinate retrieval, in which the longitude is oriented Eastward.

For each flyby, two ephemeris data files are retrieved, using the 'State Vector' WebGeoCalc capability: (a) the location of the moon and (b) that of the spacecraft, both in the *IAU_JUPITER* frame, as seen from the center of Jupiter, with a time interval of a few hours (2–4 h, depending on the spacecraft velocity relative to the moon) centered on the closest approach epoch of the flyby, and a time sampling step of 1 min. We do not correct for light time propagation. The resulting uncertainty in ephemeris data timing is of the order of 1 s, which is much below time resolution of the data and the simulations.

3. Jovian radio emissions occultations

As shown by Kurth et al. (1997), the Jovian hectometric radio emissions are occulted by Ganymede during the G01 flyby (Ganymede flyby during the first orbit around Jupiter) of the Galileo spacecraft, on June 27th, 1996. Fig. 1 of Kurth et al. (1997) shows the GLL/PWS spectrogram during G01 flyby (also displayed on the bottom-left panel of Fig. 2). The full occultation is observed between 05:50 and 06:20 SCET. The occultation spectral ingress and egress profiles imply that the observed radio sources at higher frequencies (located close to Jupiter) are occulted earlier and reappears later than the lower frequency ones, which are located farther out from Jupiter. Possible occultation of the Jovian radio emissions have been also reported during the first Io flyby of Galileo (Louarn et al., 1997).

Table 1 shows our assessment of all targeted Galilean moon flybys by the Galileo spacecraft. Appendix D provides access to the full material used to conduct this study, with figures corresponding to each flyby. In this paper, we have selected one flyby of each Galilean moon, where the radio emission occultation was clearly observed (see the grey rows in Table 1). Fig. 2 shows GLL/PWS observations for each of the selected flybys, i.e., from left to right and top to bottom: Io (I24), Europa (E12), Ganymede (G01) and Callisto (C30) flybys.

3.1. Radio emission modelling

We model the location of the Jovian auroral radio sources visible at Galileo's location using ExPRES (version 1.1.0, Louis et al., 2020)). Our simulation runs are configured as follows: (a) we use the JRM09 magnetic field model (Connerney et al., 2018) together with the Connerney et al. (1981) current sheet model; (b) the sources are set every 1° in longitude along active magnetic field lines of M-shell = 30 (M-shell being the measure of the magnetic apex, i.e., the distance in Jovian radii (R_J), of the magnetic field line at the magnetic equator; it is different from the L-shell, for which the jovigraphic equator is considered for the magnetic apex), corresponding to the main auroral oval (Grodent, 2015); (c) the unstable electron temperature is set to 5 keV (Louarn et al., 2017); and (d) the location of the visible radio sources is modelled with a temporal step of 1 min. These parameters are fixed for all simulation runs used in this study. We also included Io-induced radio emissions in the simulation runs, with the same unstable electron distribution temperature (5 keV). The ExPRES configuration files are available, as described in appendix D.

When the observer is located near the magnetic equator, the radio source beaming pattern implies that the visible radio sources are split into four cluster locations, called A, B, C and D, corresponding respectively to the North-Eastern, North-Western, South-Eastern and South-Western quadrant around Jupiter as seen from the observer (see, e.g., Fig. 2 of Marques et al., 2017, for a definition).

The simulation runs have been computed using the OPUS (Observatoire de Paris UWS Server, Servillat et al., 2021a) instance operated by PADC[4] for the MASER (Measurement, Analysis and Simulation of

[3] CReMA-3.0 trajectory information: https://www.cosmos.esa.int/web/juice/crema-3.0 (last access: 17-Aug-2021).

[4] Paris Astronomical Data Centre: https://padc.obspm.fr (Re3data record id: http://doi.org/10.17616/R31NJMS9).

Table 1
List of all targeted Galilean moon flybys with PWS/Electric-Survey data. The data from all flybys (except E18) are available through the University of Iowa *das2* server end-point. The spacecraft ephemeris data is available for all flybys except E15. The occultation assessment indicates if the occultation is observed (*yes* or *no*) or unsure *(?)*. The grey lines correspond to the flybys shown in Fig. 2 and described in detail in this study. Table adapted from Table 1 (Orbital Facts) of the CATALOG/GO_MISSION.CAT label file available from Gurnett et al. (1997).

Orbit	Moon		Data Availability		Occultation
Name	Name	Closest Approach	GLL/PWS	SPICE	Assessment
I00	Io	1995-12-07 17:45:58	yes	yes	*(?)*
G01	Ganymede	1996-06-27 06:29:07	yes	yes	*yes*
G02	Ganymede	1996-09-06 18:59:34	yes	yes	*(?)*
C03	Callisto	1996-11-04 13:34:28	yes	yes	*(?)*
E04	Europa	1996-12-19 06:52:58	yes	yes	*no*
E06	Europa	1997-02-20 17:06:10	yes	yes	*(?)*
G07	Ganymede	1997-04-05 07:09:58	yes	yes	*(?)*
G08	Ganymede	1997-05-07 15:56:10	yes	yes	*yes*
C09	Callisto	1997-06-25 13:47:50	yes	yes	*(?)*
C10	Callisto	1997-09-17 00:18:55	yes	yes	*no*
E11	Europa	1997-11-06 20:31:44	yes	yes	*no*
E12	Europa	1997-12-16 12:03:20	yes	yes	*yes*
E14	Europa	1998-03-29 13:21:05	yes	yes	*(?)*
E15	Europa	1998-05-31 21:12:57	yes	no	*yes*
E16	Europa	1998-07-21 05:03:45	yes	yes	*(?)*
E17	Europa	1998-09-26 03:54:20	yes	yes	*(?)*
E18	Europa	1998-11-22 11:38:26	no	yes	–
E19	Europa	1999-02-01 02:19:50	yes	yes	*(?)*
C20	Callisto	1999-05-05 13:56:18	yes	yes	*no*
C21	Callisto	1999-06-30 07:46:50	yes	yes	*no*
C22	Callisto	1999-08-14 08:30:52	yes	yes	*yes*
C23	Callisto	1999-09-16 17:27:02	yes	yes	*yes*
I24	Io	1999-10-11 04:33:03	yes	yes	*yes*
I25	Io	1999-11-26 03:59:15	yes	yes	*(?)*
E26	Io	2000-01-03 17:59:56	yes	yes	*no*
I27	Io	2000-02-22 13:46:36	yes	yes	*yes*
G28	Ganymede	2000-05-20 10:10:18	yes	yes	*no*
G29	Ganymede	2000-12-28 08:25:27	yes	yes	*no*
C30	Callisto	2001-05-25 11:23:58	yes	yes	*yes*
I31	Io	2001-08-06 04:59:21	yes	yes	*no*
I32	Io	2001-10-16 01:23:21	yes	yes	*(?)*
I33	Io	2002-01-17 14:08:23	yes	yes	*(?)*

Emissions in the Radio range) project (Cecconi et al., 2020). OPUS is a framework running the Universal Worker Service (UWS) protocol (Harrison and Rixon, 2016). The ExPRES code is available for open access run-on-demand from this interface.[5]

3.2. Occultation modelling

The occultation is computed using a simple geometric derivation of the intercept distance between the center of the Galilean moon and the straight lines passing by each visible modelled radio source and the observer. Any source with an intercept distance shorter than one moon radius is occulted, assuming a spherical moon, as sketched on Fig. 3.

3.3. Occultation timing uncertainty

Using the radio source location accuracy estimated in Appendix B, it is possible to estimate the uncertainty of the predicted occultation timings. Assuming the time uncertainty δt to be sufficiently small, simplifying assumptions can be made: (i) the distance d from the observer and the moon is constant; (ii) the relative velocity V between the observer and the moon is also constant, and is considered perpendicular to the line pointing to the radio source location. The angular uncertainty of the radio source location is $\delta\theta$. Fig. 4 presents this simplified scheme. The observed moon is moving by a distance $\delta r = V\delta t$ to cover the angular uncertainty interval $\delta\theta$ as seen from the observer. We can derive δt as follows:

$$\delta t \sim \frac{d\tan\,\delta\theta}{V} \tag{1}$$

With an angular uncertainty of the order of 1° (see Appendix B), the previous equation evaluates as: $\delta t \sim 0.02$ d/V. This simplified estimation scheme corresponds to the worst case scenario. This measure of the uncertainty should thus be to taken as an upper limit.

[5] UWS MASER portal: https://voparis-uws-maser.obspm.fr/client/.

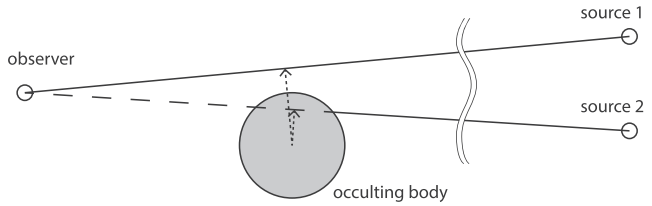

Fig. 3. Simple geometric occultation scheme used in this study. The interception distance (dotted segment) is computed as the distance between the center of the occulting body and the line of sight between the observer and the source. In this case the source 1 is not occulted, while source 2 is.

4. Observations

All Galileo flybys have been analysed and modelled using ExPRES. In this section, we present the detailed modelling results corresponding to the highlighted rows of Table 1. Figs. 5–7 and 9 present the results for these four flybys. The flybys are presented in order to show the simpler to the more complex cases. The GLL/PWS data (same data as in Fig. 2) are plotted together with the simulations of observable auroral radio emissions (described in Section 3.1) separated into the four source types A, B, C and D (from white to black, respectively). The comparison of observations and modelled data shows that the simulations reproduce the Jovian radio occultation during the four flybys presented in Fig. 2.

Appendix D describes the supplementary material available for all flybys (Cecconi et al., 2021), which contains all the material used to conduct this study. For each Galileo flyby, we provide: (a) a figure showing the GLL/PWS data and the observable radio sources modelled by ExPRES, and (b) movies showing a subset of Jovian radio sources (a selected sub-set of frequencies), as seen from Galileo ('pov' movies), or from the top of the Jovian system ('top' movies).

4.1. Callisto C30 flyby

The occultation occurring during the C30 flyby of Callisto is displayed in Fig. 5. The ingress occultation time is very well reproduced (within 1 min accuracy). All sources are occulted simultaneously, with radio emissions intensity dropping instantly, at ~11:25 SCET. At egress, we observe first a faint rise of the emission intensity from ~11:50 to ~12:00, and then a sudden return to maximum intensity at ~12:00. This egress phase can be visualised in the supplementary material available for this flyby: https://doi.org/10.25935/8ZFF-NX36#C30. The frames between 11:44 to 11:59 of the 'pov' movie clearly shows the various sources reappearing one after the other: first, the B sources, then the A and D sources simultaneously and finally the C sources. The predicted reappearance of C sources perfectly coincides with the observed full egress phase. This leads to two observations: (i) the main radio contribution is that of the C sources at the time of observation, and (ii) the radio sources are occulted by the moon's surface (or very close to it).

The low-frequency cut-off is not perfectly modelled (especially on the ingress side), with a shift of about 200 kHz with respect to the observations. The error of a few 10s–100 s kHz is probably due to an incorrect estimation of the electron density around Jupiter. In addition to this

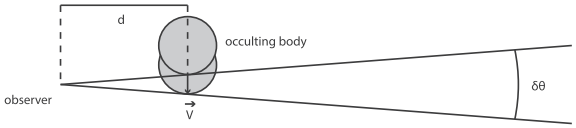

Fig. 4. Simple flyby geometry used to evaluate the occultation timing uncertainty. The observer is noted "S/C". V is the relative velocity of the observed moon with respect to the observer. d is the distance of the observer to the moon. $\delta\theta$ is the angular uncertainty of the radio source location.

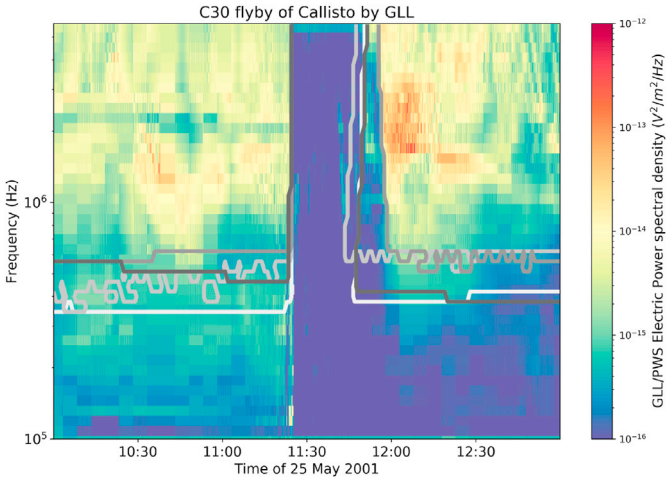

Fig. 5. Superimposed GLL/PWS data and ExPRES simulations during Jovian radio emission occultations by Callisto (flyby C30). The four types of emission (A, B, C, D) are separated (from white to dark grey, resp.).

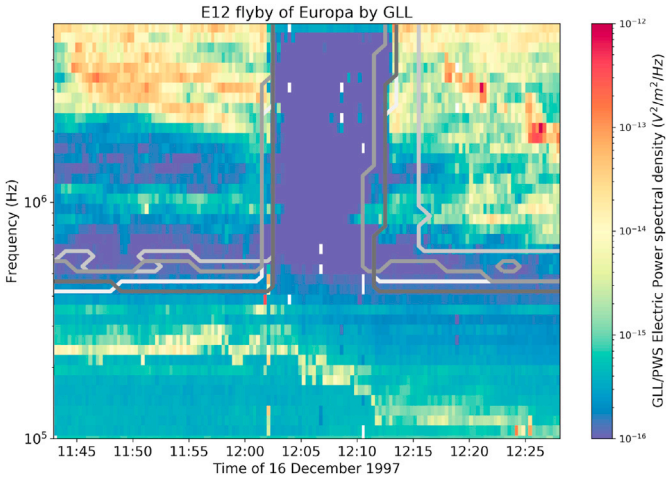

Fig. 6. Superimposed GLL/PWS data and ExPRES simulations during Jovian radio emission occultations by Europa (flyby E12). The four types of emission (A, B, C, D) are separated (from white to dark grey, resp.).

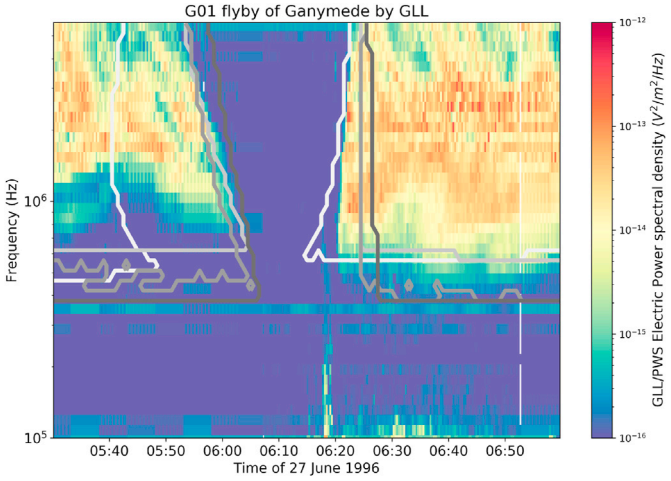

Fig. 7. Superimposed Galileo PWS data and ExPRES simulations during Jovian radio emission occultations by Ganymede (flyby G01). The four types of emission (A, B, C, D) are separated (from white to dark grey, resp.).

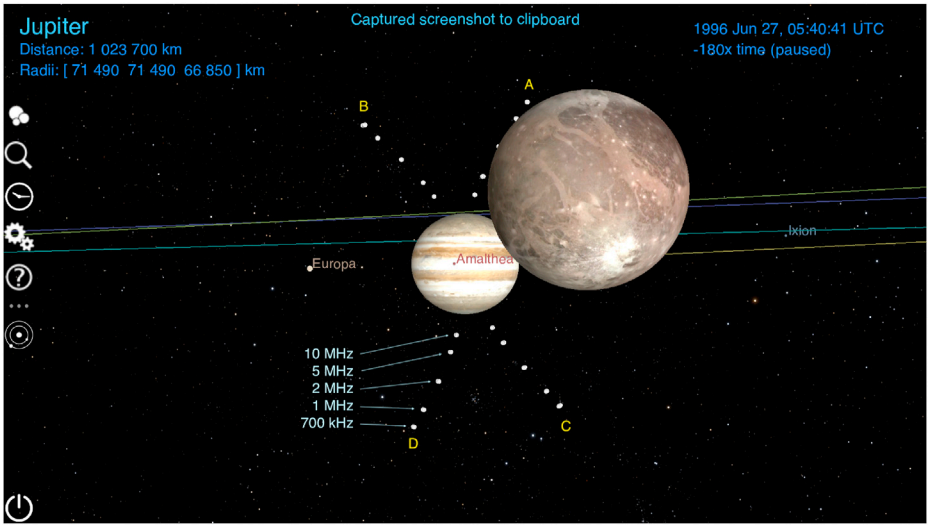

Fig. 8. G01 Flyby visualised in the Cosmographia tool. The scene is set with an observer on the Galileo spacecraft, pointing to Jupiter. Ganymede is in the field of view. The ExPRES-modelled visible radio sources are also shown, at 700 kHz, 1 MHz, 2 MHz, 5 MHz and 10 MHz. The radio sources are naturally grouped in four sets (named A, B, C and D). A the time of the snapshot (1996-06-27T05:40:41 SCET), the ingress phase is starting, with the occultation of radio sources at 2 MHz in the A-group.

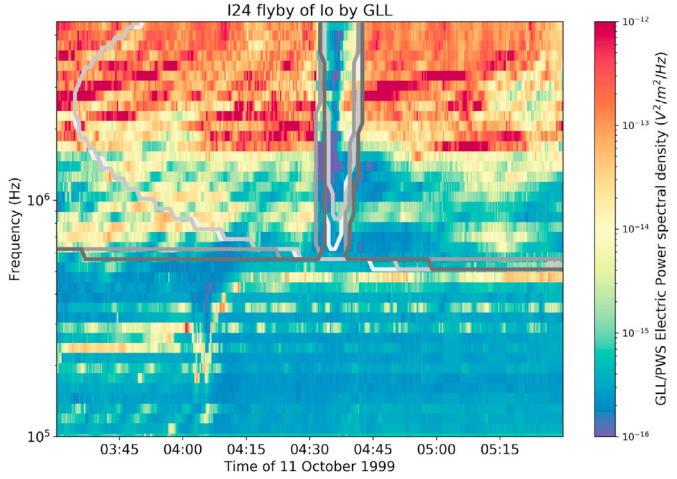

Fig. 9. Superimposed GLL/PWS data and ExPRES simulations during Jovian radio emission occultations by Io (flyby I24). The four types of emission (A, B, C, D) are separated (from white to dark grey, resp.).

spectral shift, some components show an erratic cut-off line shape (B sources –light grey– throughout the interval, except during the occultation, and C sources –medium grey– after the occultation). It is not fully understood why and under which conditions, some components show a rather stable cut-off line, and some other a more erratic one. However, it is noticeable that the erratic features of the B sources cut-off line look like the lower end of vertex-early arcs (e.g., at ~10:10, ~10:25 or ~11:45), and those of the C sources look like those of vertex-late arcs (e.g., at ~12:15).

An attenuation feature is observed starting at ~2.5 MHz, and decreasing to ~2 MHz at ingress. This corresponds to the attenuation lanes described in Section 1. In addition, during the full occultation period of time, unexpected faint and sporadic signals are observed between ~800 kHz and ~2 MHz.

4.2. Europa E12 flyby

The E12 Europa flyby (Fig. 6) is similar to C30 Callisto's flyby case, where all sources are occulted simultaneously at ingress. Faint and sporadic radio signatures are observed during the full occultation phase (as in the case of C30). At egress, the simulation well reproduces the end of the occultation, except in the ≃ [800–1000] kHz frequency range where we observed emission during the modelled occultation. The full E12 flyby data is available at: https://doi.org/10.25935/8zff-nx36#E12.

The attenuation lane feature is observed at and below ~2 MHz before ingress, with a corresponding feature after egress, up to ~12:20. At about ~1 MHz, an intensification is also observed, before ingress and after egress (corresponding to the aforementioned prediction mismatch), and is probably linked to the attenuation lanes.

The spectral line observed between ~250 kHz (at the beginning of the interval) and ~100 kHz (at the end) corresponds to the local plasma upper-hybrid frequency line ($f_{UH} = (f_{pe}^2 + f_{ce}^2)^{1/2}$, with f_{pe} and f_{ce}, the plasma frequency and the electron cyclotron frequency, respectively).

4.3. Ganymede G01 flyby

Fig. 7 displays the occultation modelling of the Jovian radio emissions during the G01 flyby of Ganymede. At ingress, unlike the previous two cases, all sources are not occulted simultaneously. First the A sources are occulted, then the B, C and D sources, with the beginning of the full occultation. Before observed egress, a broadband noise burst at ~06:18, going up to ~800 kHz. This has been interpreted as the signature of Ganymede's magnetopause crossing by Gurnett et al. (1996). At egress, the modelled reappearance of the A sources (white line) well reproduces the end of the observed occultation at frequencies higher than a few MHz. At lower frequencies, the egress occurs later than predicted. At ~ 700 kHz, it is observed at ~06:21, and predicted at ~06:16. This mismatch is likely due to refraction of radio waves in Ganymede's atmosphere or ionosphere.

During this flyby, the radio sources are not occulted simultaneously at both egress and ingress, and not at the same time on the whole spectral range, which is due to the trajectory of Galileo. Fig. 8 shows a modelled image, from the Galileo spacecraft point of view, at the beginning of the G01 occultation sequence. This frame is extracted from the G01 movie available in supplementary material at: https://doi.org/10.25935/8zff-nx36#G01.

4.4. Io I24 flyby

Fig. 9 displays the occultation during the I24 Io's flyby. At ingress, the occultation of the higher intensity is well modelled. We observe radio signals during the modelled full occultation, and the observed egress seems to occur earlier than the prediction. Intense radio arcs are visible above 2 MHz, showing the lower frequency part of vertex-late arcs. The radio signal is attenuated below 1–2 MHz, especially after the flyby. The f_{UH} line is also observed (~300 kHz to ~500 kHz). The full I24 flyby data is available at: https://doi.org/10.25935/8zff-nx36#I24.

This Io flyby also shows a noticeable feature. The modelled Northern

radio sources (A and B, respectively in white and light-grey) are not observed at the beginning of the studied interval. This is due to the "Equatorial Shadow Zone" (ESZ) effect reported at Saturn (Lamy et al., 2008), see Appendix A for more details.

4.5. Other flybys

In the case of flybys with partial occultations (e.g., G02, G07, E11, E26 or G28), the Jovian radio signals are observed during the flyby, with no full occultation interval. During the G07 flyby, only D sources are occulted. The GLL/PWS data (see https://doi.org/10.25935/8zff-nx36#G07) shows an attenuation of the Jovian radio signals that fits the predicted occultation (see Fig. 10), hence suggesting that several radio sources were active, including the D sources.

Most of the other flybys (e.g., C03, E04, E06, G08, C10, E19) are occurring on the Jovian-facing side of the moon, where no occultation can occur.

5. Results and discussion

5.1. Temporal occurrence and spectral coverage of Jovian auroral radio signals

The first result of this study is the fact that Jovian auroral radio emissions are present almost continuously, although this may not be obvious in some observational data sets, due to the limited sensitivity of instruments. Ground based radio telescopes (such as the Nançay Decametre Array, in France) provide the longest observation collections (Marques et al., 2017), but the distance to Jupiter limits the detection of low intensity events despite their intrinsic sensitivity. Space borne radio instruments (such as Voyager/PRA, Cassini/RPWS, GLL/PWS or Juno/Waves), provide observations from a closer range to Jupiter. Cassini and Galileo data show quasi-continuous radio signals (as shown on Fig. 1). The ExPRES modelling of auroral radio sources, configured with radio sources every 1° in longitude, is consistent with this observation (with the noticeable exception of the ESZ, for an observer located around Io's orbital distance to Jupiter).

The occultation modelling analysis shows that all sources must be occulted at the same time in order to remove the natural radio signature of Jupiter's magnetospheric activity. It is also noticeable that faint emissions are still visible during some occultations (e.g., during the G01, E12 and C30 Galileo flybys).

The JUICE/RPWI and RIME instruments will observe in the same radio environment. The JUICE/RIME and Cassini/RPWS instruments have similar antenna characteristics, leading to an antenna resonance at about ~9 MHz (Zarka et al., 2004; Bruzzone et al., 2013). It is thus very likely that JUICE/RIME will observe similar signals as those shown on Fig. 1 (with a spectral range restricted around 9 MHz).

The low frequency limit is usually well predicted by ExPRES, as shown on Figs. 5–7, 9 and 10. The ExPRES low frequency emission limit is determined by the CMI theory: the emission can occur only when $f_{pe}/f_{ce} < 0.01$. This finding implies that our modelling of the magnetic field and plasma density is consistent with the radio observations. Discrepancies (e.g., during flyby C30) may be related to the modelling of the two aforementioned characteristic frequencies: f_{pe} depends on the magnetospheric current sheet model; and f_{ce} is determined by the magnetic field model. The JRM09 magnetic field model is derived from the Juno magnetic measurements in the polar regions of Jupiter. This model is thus perfectly adapted for our application. Conversely, the current sheet model could be improved. The results of this study will be checked and updated if required when the new Connerney et al. (2020) model is included into ExPRES. The effect of the Solar Wind conditions may also play a role (as studied by Hess et al., 2012) at the lowest frequencies.

5.2. Radio source location

Fig. 11 displays the occultation of the Jovian radio sources during the flyby I24, for two sets of simulation runs. In the top and bottom panels, the sources are located on the magnetic field lines with an M-shell of 50 and 30 R_J, respectively, with the larger M-shell, corresponding to radio sources located at higher magnetic latitudes. We observe no difference for the occultation prediction. This finding implies that updating the current sheet model (Connerney et al., 2020) should have a limited impact on the results of this study.

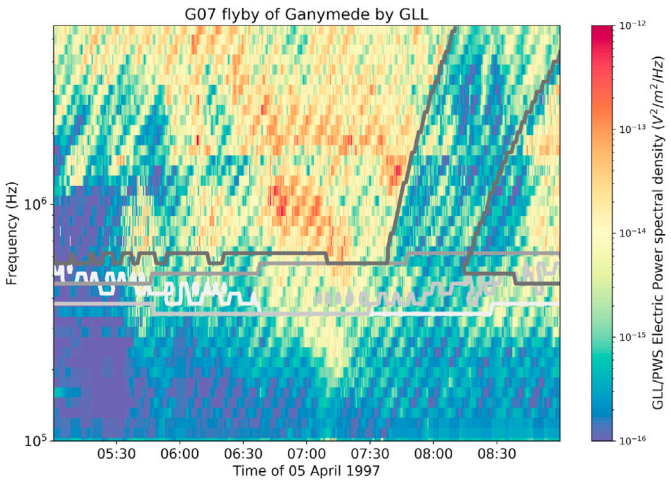

Fig. 10. Superimposed Galileo PWS data and ExPRES simulations during Jovian radio emission occultations by Ganymede (flyby G07). The four types of emission (A, B, C, D) are separated (from white to dark grey, resp.).

The difference in the low cut-off frequency of the simulated emissions is very small (with a slightly lower low cut-off frequency for sources with M-shells of 50 R_J). The main difference is observed for the A and B sources (white and light-grey curve), with the ESZ feature occurring at a different time.

An assessment of the radio source location prediction accuracy is presented in Appendix B. We show that the overall angular accuracy of the radio source location is below 1° at 10 MHz for observations at Europa, Ganymede and Callisto. The 1° accuracy threshold is met at 5 MHz at Europa, 2 MHz at Ganymede, and 700 kHz at Callisto. See Table B5 for detailed results.

5.3. Occultation modelling accuracy and propagation effects

The ExPRES modelling accurately predicts the observed occultation (e.g., C30 flyby, or E12 and I24 flyby ingress). The ExPRES simulation runs have been configured with a 1 min sampling step, which sets the general temporal sampling of this study. Table 2 shows the modelled occultation timing accuracy, using Equation (1). All values are below 1 min, justifying the 1 min sampling precision used in this study. The discrepancies between the predictions and observation have to be further studied. The mismatch mostly occurs at frequencies lower than ~1 MHz. In this range, propagation effects (such as refraction effects) are known to occur, with, e.g., attenuation lanes. We observe them in all studied flybys, e.g., on E12, where the Jovian auroral radio waves are attenuated below ~2 MHz, with an intensification at ~1 MHz.

In the case of G01, the egress is observed several minutes after the predicted egress time. Since refraction in the moon's atmosphere and ionosphere is bending away optical paths (see, e.g., Colin, 1972), the apparition of the source at egress is observed later than compared to the straight line propagation case. Fig. 12 shows how the same observations can be interpreted considering refraction effects on the ionosphere of the moon.

In Figs. 5–7, we observe faint and sometimes sporadic radio signals, which are visible during the occultation interval, despite the predicted full occultation. Since the moon is geometrically occulting all the Jovian radio sources, refraction effects must be taken into account to interpret the observation. These effects can occur either in the moon's atmosphere

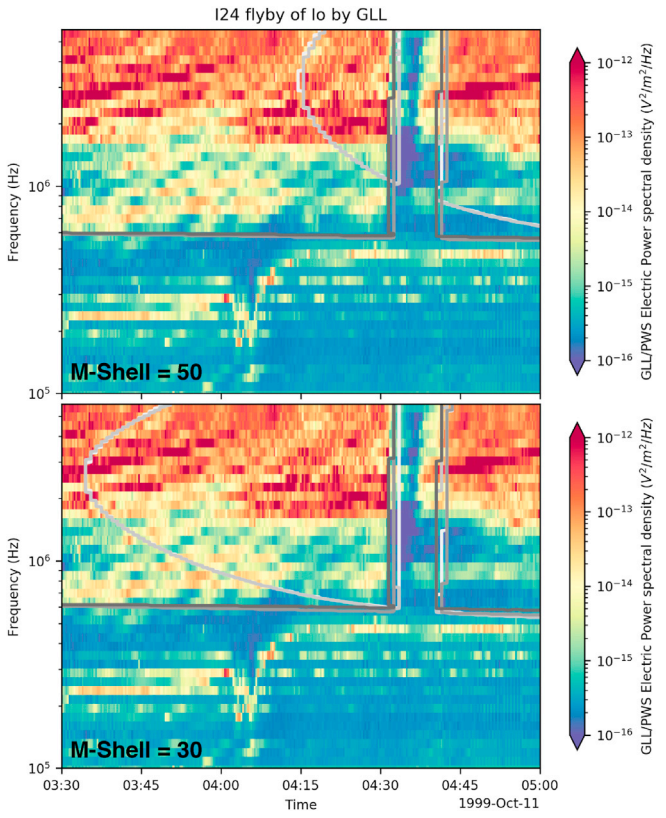

Fig. 11. Comparison between the Jovian radio occultation during the I24 flyby for sources on magnetic field lines at M shell M = 50 (top panel) and M = 30 (bottom panel).

Table 2
Estimation of the temporal uncertainty of the predicted occultation timing in seconds.

Flyby	Phase	Date Time (SCET)	Temporal accuracy (s)				
G01	ingress	1996-06-27 06:00:00	55	45	32	19	13
G01	egress	1996-06-27 06:20:00	22	18	13	7	5
E12	ingress	1997-12-16 12:02:00	14	12	8	5	4
E12	egress	1997-12-16 12:12:00	29	24	17	11	8
I24	ingress	1999-10-11 04:33:00	23	19	14	9	6
I24	egress	1999-10-11 04:42:00	49	40	28	18	12
C30	ingress	2001-05-25 11:25:00	5	4	3	1	1
C30	egress	2001-05-25 11:50:00	26	20	15	8	5
Frequency (MHz)			0.7	1.0	2.0	5.0	10.0

and ionosphere, in the Io plasma torus or in the magnetospheric plasma sheet. ExPRES assumes a straight line propagation between the radio source and the observer.

The two latter results (occultation ingress and egress prediction mismatch and faint signals during full occultation) indicate that propagation effects play an important role in the fine understanding of the Galilean radio occultations. Further analysis requires the coupling to a ray-tracing code, such as ARTEMIS-P (*Anisotropic Ray Tracer for Electromagnetism in Magnetosphere, Ionosphere and Solar wind including Polarization*, Gautier et al., 2013).

Appendix C is presenting a preliminary study estimating the range of parameters (e.g., altitudes above the surface, or plasma densities), in which the refraction effects are likely to occur. The estimation is based in the currently available Galilean moon's ionosphere models (see Table C6). Using those environment models, the refractive index is computed, using the Appleton-Hartree equation (see Equation C.1). From Fig. C18 and Equation C.2, we can derive rough estimates of the accessible parameter space with observations at each of the observation frequencies used in this study, as shown in Table C7. A first conclusion of this estimation is that no significant refraction is expected at 10 MHz at Europa, Ganymede and Callisto, so that the simple occultation modelling presented in this study should be applicable around this frequency.

6. Usage for the JUICE mission planning tools

The science planning activity, coordinated by the JUICE Science Operations Center (JUICE SOC), relies on the identification, at each point in time, of the science observation opportunities, using science models or/and geometry. For JUICE, some of those opportunities depend on the Jupiter Radio emission simulation. Ionosphere characterisation, active and/or passive radar sounding activities opportunities can benefit from an accurate simulation of Jupiter radio emission.

Since the ExPRES code can provide as by-products the locations of the radio sources as seen from the spacecraft for a range of frequencies (i.e., 1–40 MHz), the JUICE SOC has implemented a standalone tool, which wraps the ExPRES code and identifies science opportunity windows based on the radio source position. This can be used to identify opportunity windows for one of the high priority science objectives of the JUICE RPWI instrument, the icy moon ionosphere characterisation through ionosphere refraction/distortion measurement.

The opportunity periods currently generated to drive the corresponding RPWI measurements are linked to the ingress and egress occultation events of the Jupiter radio sources, where at least one Jupiter radio sources reaches JUICE with a frequency between 0.1 and 5 MHz crossing the moon ionosphere (with a thickness of ~100 km).

In Fig. 13, the Jupiter auroral radio source as seen from JUICE during 21C13 (the last Callisto flyby of the tour) as a function of frequency (MHz) and UTC time is displayed: the red dots correspond to opportunity for ionosphere characterisation, i.e., whenever one of the radio source types (A, B, C or D) is seen by JUICE with a line of sight passing through

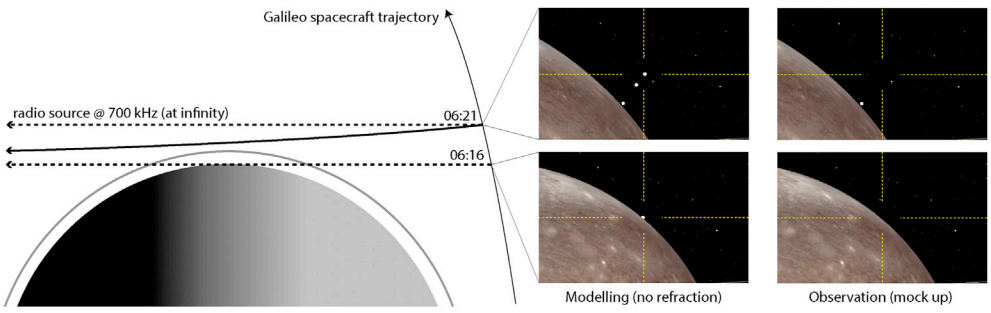

Fig. 12. Sketch of G01 configuration, with a modelled radio source at 700 kHz, assumed to be at infinity on the left-hand side. The plain line is a sketched refracted ray path. The plain grey line represents the ionosphere of the moon. The dashed lines are the straight line propagation (no refraction) for the same source. Two locations of the Galileo spacecraft trajectory are illustrated on the right-hand side of the Figure. The "Modelling (no refraction)" column shows frames extracted from the G01 'pov' movie at 06:16 and 06:21. The right-most column ("Observation") shows a mock-up of the radio source observations, including refraction effects at low frequencies.

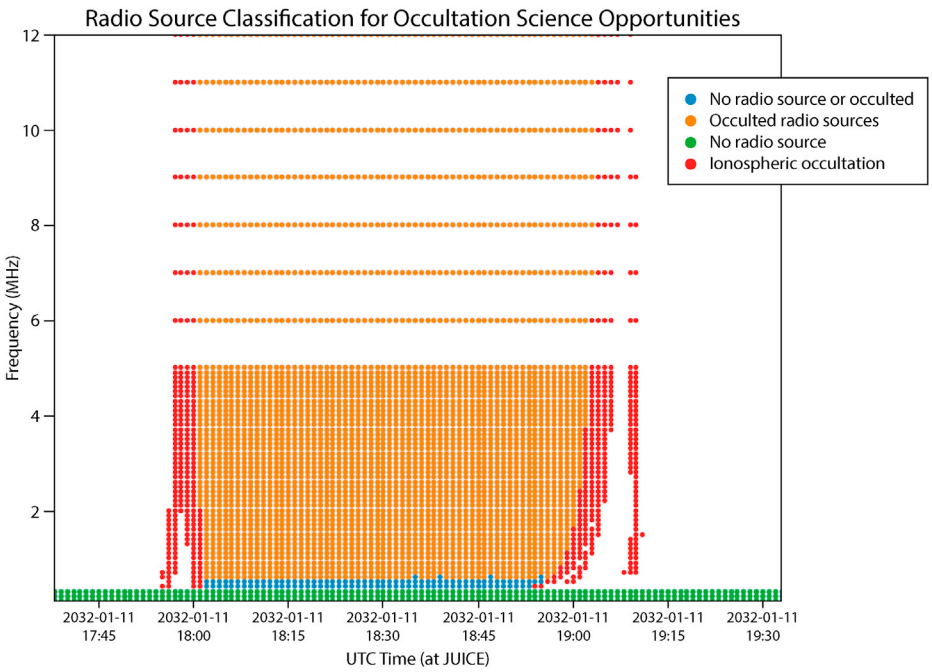

Fig. 13. Classification of observation opportunities during the last Callisto flyby (21C13) of orbital scenario CReMA 3.0. The color coded dots represent the Jupiter auroral radio source occultation state as a function of time and frequency. Red dots means that at least one of the source type (A, B, C and D) is visible from JUICE and that the line of sight between the source and the spacecraft goes through the ionosphere within 0–100 km altitude above Callisto surface. The blue, orange and green dots mean that no radio source is visible by JUICE at those frequency ranges. Here "No Radio Source" means that no signal from Jupiter radio sources should be observed: either because JUICE is outside the beam of all modelled radio sources, or because the model predicts that the radio source can't produce radio waves (e.g., in the lower frequency range).

the ionosphere within 0–100 km. This section is using the CReMA 3.0 trajectory scenario.

Fig. 14 shows the resulting ionospheric characterisation opportunities as a function of the JUICE spacecraft altitude in km (green background). There are a few gaps within the ingress and egress ionospheric characterisation opportunities. Those gaps of 1–2 min are ignored to compute the final iono_ingress and iono_egress envelops used for the observation planning. Table 4 lists the RPWI in-situ and radio measurement sequence for the 21C13 scenario based on the Closest Approach (CA), and the ingress and egress windows envelope for ionosphere characterisation. Using equation (1), we can estimate the uncertainty of the occultation timing (see Table 3).

Finally, Fig. 15 is a screenshot of this measurement sequence as shown by the JUICE SOC Mapping and Planning Payload Science software (MAPPS), used to simulate the spacecraft and payload resource status (i.e., power, data rate, on-board solid-state mass memory (SSMM)). The RPWI operations are planned around the CA and around ingress and

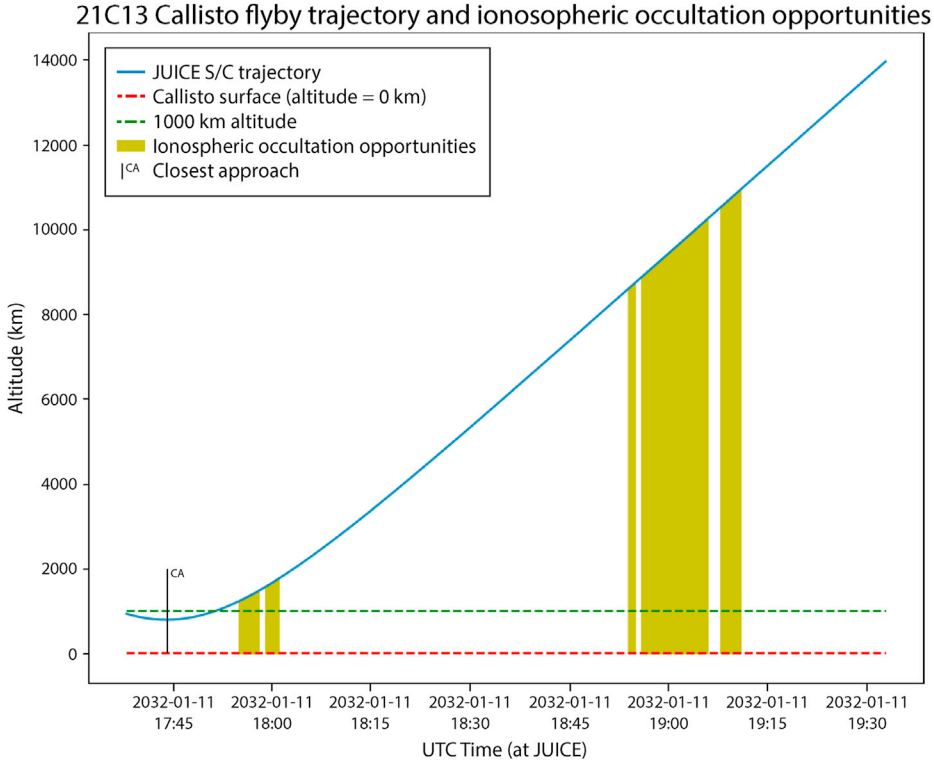

Fig. 14. JUICE spacecraft altitude above the surface of Callisto in km for the 21C13 Flyby (blue line); Callisto's surface (resp. the 1000 km altitude above surface) is represented by the red dashed line (resp. green dashed line), and the ionosphere characterisation opportunities windows are filled in green background. The figure only shows the outbound part of the 21C13 flyby, since the radio occultation opportunities are only present during this phase.

Table 3
Full occultation events at 10 MHz for JUICE flyby 21C13 of Callisto, with spacecraft altitude, relative velocity, and occultation timing uncertainty.

Event	Date Time (SCET)	Frequency (MHz)	Altitude (km)	Velocity (km/s)	Uncertainty (s)
Full Occ. Start	2032-01-11 18:00:22	10.0	1686.7	2.88	5
Full Occ. End	2032-01-11 19:03:22	10.0	9880.1	2.45	18

Table 4
RPWI in-situ and radio observations mode sequence during the 21C13 Callisto flyby scenario. Some mode changes are scheduled w.r.t. Closest Approach event (CA), while ionosphere characterisation observations are scheduled w.r.t. ingress and egress events as identified using Express. The last two column indicates which operating mode is for the *In-situ* or *Radio* sub-systems of RPWI. Each mode has a specific data rate, as well as a specific power consumption. Without explaining the details of each modes, this table shows how the various modes are activated sequentially.

UTC Date & Time	Reference Event	Relative Time	In-situ	Radio
2032-01-11T05:44:05	CA	− 12:00:00	slow	full
2032-01-11T08:14:05	CA	− 09:30:00	normal	full
2032-01-11T17:34:05	CA	− 00:10:00	burst	full
2032-01-11T17:54:05	CA	+ 00:10:00	normal	full
2032-01-11T17:55:00	iono_ingress	+ 00:00:00	normal	burst
2032-01-11T18:01:00	iono_egress	+ 00:00:00	normal	full
2032-01-11T18:54:00	iono_ingress	+ 00:00:00	normal	burst
2032-01-11T19:11:00	iono_egress	+ 00:00:00	normal	full
2032-01-12T03:14:05	CA	+ 09:30:00	slow	full
2032-01-12T05:44:05	CA	− 12:00:00	slow	full

egress ionosphere characterisation opportunities as described in Table 4. The high-resolution in-situ measurement mode is scheduled ± 10 min around the closest approach (CA), while the high resolution radio measurement mode is scheduled during the ionosphere characterisation opportunities. High-resolution modes are the most demanding in term of resources (power, data generated, stored in SSMM and to be downloaded (data rate)) and they are reserved for priority scientific objectives. So it is crucial to be able to calculate the corresponding opportunities windows.

The JUICE mission is in development phase, with a planned launch in September 2022. At this stage the JUICE mission science planning process is being exercised by analysing representative science scenarios similar to 21C13. In this study, the scenario analysis covers ±12 h around the Callisto closest approach. Fig. 15 shows the full interval, while Figs. 13 and 14 are focusing on the time interval displaying radio occultation events. The JUICE SOC will identify the same type of opportunity windows whenever a new candidate trajectory is available for JUICE.

The ExPRES simulation results can also be useful for other types of measurement, and will be made available for JUICE SOC instrument teams. This includes the measurement linked to the icy shell characterisation of the icy moons:

- Passive radar measurement by RIME or by RPWI: Opportunities can be identified whenever any radio source is visible from the spacecraft for any source type (A, B, C or D), and per source type (to differentiate source from northern and southern hemispheres) between 1 and 40 MHz (although lower frequencies are better since they allow to probe deeper layers of the icy shells);
- Active Radar measurement by RIME: when the spacecraft is protected from Jupiter radio emission due to moon occultation for sources with frequency between 9 and 11 MHz (i.e., flybys and Ganymede phase) and when the spacecraft is within the RIME instrument operating range (altitude <1000 km).

7. Conclusions and perspectives

The Galileo radio occultations observed in the PWS data set are well modelled by ExPRES simulation, with a sampling of the order of 1 min. Discrepancies between predicted and observed ingress or egress times can be attributed to refraction effects, which are not included in the current modelling scheme. The validation on GLL/PWS data allows us to apply the same modelling to the JUICE mission planning, in order to support the scientific segmentation of the Galilean moon flybys. The ExPRES modelling will also be useful for data analysis of "passive radar" observations, since it provides the location of the Jovian radio sources used to probe the moon's sub-surface.

On a technical point of view, the JUICE modelling have been done running ExPRES through the PADC operated UWS interface based on OPUS. This framework is fully adapted to the usage presented in this study. Future developments of the ExPRES code and its implementation at PADC will include better management of Provenance metadata (Servillat et al., 2020, 2021b), to enhance the scientific traceability and reproducibility of the results.

Several means of refining the occultation modelling have been identified. The main one is involving ray-tracing in the Jovian system (mainly the Io Torus) and the moon's environment. This extra modelling step requires models of the magnetic field and plasma density environments in the vicinity of the studied moon, including the magnetospheric and moon contributions (see, e.g., Modolo et al., 2018). A second order improvement may also be provided by the use of a more accurate magnetospheric current sheet model, which will refine the location of the radio sources on the low frequency end.

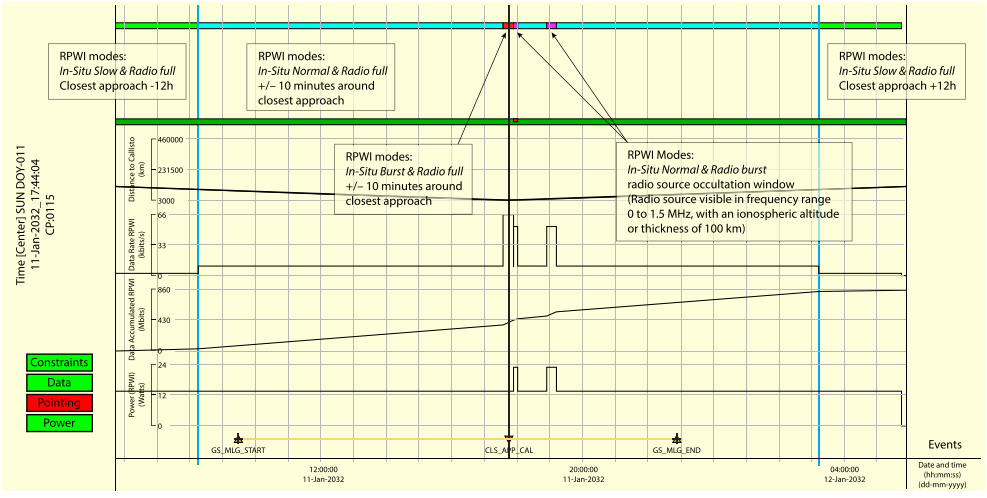

Fig. 15. Screenshot of the MAPPS interface for JUICE/RPWI during 21C13. This tools displays the various science segments, together with system parameters, such as: the distance to Callisto; the data rate produced by RPWI; the cumulated data produced by RPWI; and the instantaneous power used by RPWI. The top line is colour coded to reflect the different modes used by RPWI during the sequence. The annotations in the boxes have been added manually for this figure, and include also the *In-situ* modes, which includes others RPWI subsystems, such as the Langmuir probes or the triaxial magnetic search coil.

Author statement

Baptiste Cecconi: Conceptualization, Methodology, Software, Validation, Visualization, Writing-Original Draft, Writing-Review & Editing, Data Curation.

Corentin Louis: Conceptualization, Methodology, Software, Validation, Visualization, Writing-Original Draft, Writing-Review & Editing.

Claudio Munoz Crego: Conceptualization, Software, Validation, Visualization, Writing-Original Draft, Data Curation.

Claire Vallat: Conceptualization, Writing-Review & Editing.

Declaration of competing interest

The authors declare that they have no known competing financial interests or personal relationships that could have appeared to influence the work reported in this paper.

Acknowledgments

The authors acknowledge support from Observatoire de Paris–PSL, CNRS, CNES and ESA for funding the research. CKL's work at DIAS is supported by the Science Foundation Ireland Grant 18/FRL/6199. The authors also acknowledge support from the Europlanet 2024 Research Infrastructure (EPN2024RI) project, which has received funding from the European Union's Horizon 2020 research and innovation programme under grant agreement No 871149). They want to emphasise the use of community developed tools and standards, which greatly facilitated this study (such as Autoplot, Das2, OPUS, UWS and Cosmographia and WebGeoCalc). They thank PADC for providing computing and storage resources. The authors thank Ronan Modolo for fruitful discussions during the preparation of the manuscript. They also thank Marc Costa (from the NAIF SPICE team at NASA/JPL) for his very helpful feedback on configuring and using Cosmographia.

Appendix A. Equatorial Shadow Zone

In the equatorial region, in the innermost magnetosphere, the auroral radio sources are not visible, due to combination of the shape of the radio emission beaming patterns and the topology of the magnetic field lines bearing the radio source. This effect is named "Equatorial Shadow Zone" (ESZ). This effect has been identified at Saturn (Lamy et al., 2008), using a preliminary version of the ExPRES code. It has also been observed at Earth (see, e.g., Morioka et al., 2011, Fig. 1), but not explicitly described.

Our simulation runs show that some of the Jovian auroral radio sources are not always visible at the distance of Io's orbit. Fig. A.16 shows the observability for each auroral radio source for an observer located on Io's orbit, during one rotation of Jupiter. The simulation shows that the Southern radio sources (namely, the C and D source) are not visible in the CML range 180–210°. The Northern radio sources (namely, the A and B source) are observable from all CML, with a drastically reduced spectral range at a CML of about 25°. Since the Northern and Southern ESZs do not occur at the same time, an observer will not experience a full dropout of radio signals, contrary to what is observed at Saturn.

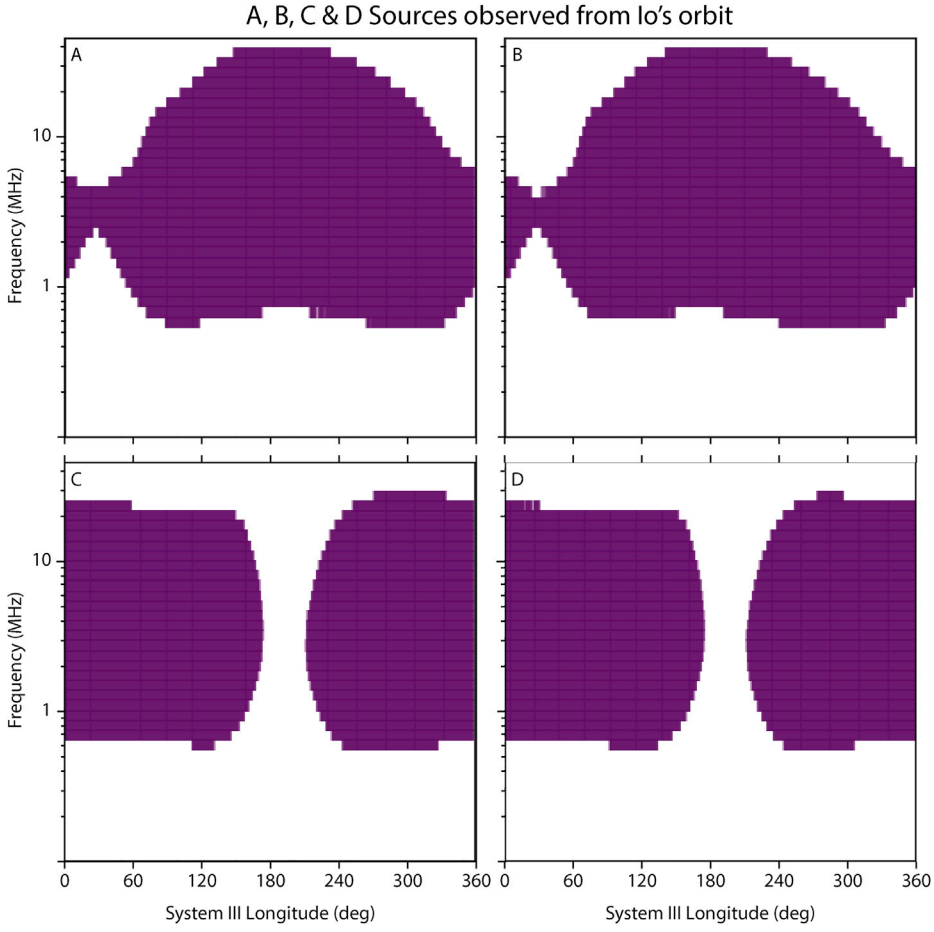

Fig. A.16. Jovian auroral radio source observability from Io's orbit.

Appendix B. Radio source location uncertainty

The ExPRES code provides the observable radio source locations, given a series of input parameters (Jovian magnetic field model, Jovian current sheet model, electron population properties in the radio source). The main source of uncertainty on the radio source location is the selected M-shell of the magnetic field line bearing the radio sources. Louis et al. (2019b) identified radio sources on M-shells between 10 and 50 Jovian radii. We thus use this range of values to evaluate the variation of radio source location. Fig. B.17 shows the variation of the radio source locations, at five selected frequencies, for all longitudes. We use this estimation to derive the angular uncertainty of the radio source location, as observed from the Galilean moons, as presented in Table B.5. For instance, at 10 MHz, the error on the source position, is below 1° at Europa, Ganymede and Callisto.

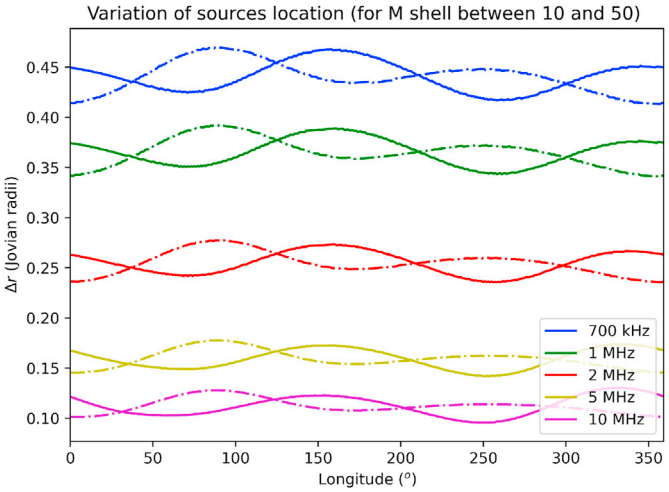

Fig. B.17. Radio sources location shifts (in Jovian radii) with varying M-shell (from 10 to 50 R_J), as a function of longitude, for the Northern (solid line) and Southern (dotted-dashed line) hemispheres, at different frequencies: 700 kHz (blue), 1 MHz (green), 2 MHz (red), 5 MHz (yellow) and 10 MHz (purple).

Table B.5
Angular uncertainty (in degrees) of Jovian radio sources location for M-shells, as observed from each Galilean moons and for a set of 5 frequencies from 700 kHz to 10 MHz).

	Angular uncertainty (deg)				
Moon	700 kHz	1 MHz	2 MHz	5 MHz	10 MHz
Io	4.3	3.5	2.5	1.6	1.1
Europa	2.7	2.2	1.6	1.0	0.7
Ganymede	1.7	1.4	1.0	0.6	0.4
Callisto	1.0	0.8	0.6	0.3	0.2

Appendix C. Evaluation of refraction effects

The impact of propagation effects on the low frequency radio waves in the Galilean moon environments can be evaluated using the currently available plasma environment models (see Table C.6). Using these models, the refraction index is computed after the Appleton-Hartree equation (Appleton, 1932), which defines the refractive index for electromagnetic wave propagation in a cold and magnetised plasma:

$$n^2(\omega) = 1 - \frac{2X(1-X)}{2(1-X) - Y^2\sin^2\theta \pm \sqrt{Y^4\sin^4\theta + 4(1-X)^2Y^2\cos^2\theta}} \tag{C.1}$$

with n the refractive index, $X = (\omega_p/\omega)^2$, $Y = \omega_c/\omega$, θ is the propagation angle (between the wave vector and the local magnetic field vector), and sign of $\pm$ is the propagation mode. The X term is computed using the selected plasma density models. The Y is evaluated using the average value of the Jovian magnetic field strength at each moon, that are 400 nT, 120 nT and 30 nT, for Europa, Ganymede and Callisto respectively. In the case of Ganymede, two cases have been studied, with the surface magnetic field values at the equator of the moon (720 nT) and at its poles (1440 nT). In all cases, the Y^2 value is negligible compared to the order of magnitude of X, except very close to the moon surface. In turn, the variation with angle θ is also negligible. We thus only show figures for $\theta = 0$ with the $+$ propagation mode and the local Jovian magnetic field strength, except for the case of Ganymede, where we considered the polar magnetic field strength.

It is noticeable that setting $Y = 0$ simplifies Eqn C.1 to:

$$n^2(\omega) = 1 - X = 1 - \left(\frac{\omega_p}{\omega}\right)^2 \tag{C.2}$$

So that the refractive index only depends on the plasma frequency and the radio wave frequency. Table C.7 presents estimated lower plasma density limit and upper altitude limits for various observations frequencies at Europa, Ganymede and Callisto. These estimates are computed using Eqn C.2 and the various environment models presented in this section.

Fig. C.18 shows the squared refractive index value n^2 iso-contours in the plasma density versus frequency or altitude versus frequency spaces. These plots can be used to evaluate in which regimes the refraction effects will be observable. We consider that the $n^2 = 0.99$ contour provides a rough upper

limit of this domain. Hence, for instance, with an observation frequency of 2 MHz at Europa, refraction effects are likely to occur up to ~ 700 km above the surface, or at plasma densities above ~ 500 cm^{-3}, confirming the rough estimate provided in Table C7.

Table C.6
Plasma environment model parameters (reference density n_0 and scale height h_0) for Europa, Ganymede and Callisto.

Moon	n_0 (cm^{-3})	h_0 (km)	Reference
Europa	9000	250	Kliore (1998)
Ganymede	400	600	Gurnett et al. (1996)
Ganymede	2200	125	Eviatar et al. (2001)
Callisto	10000	30	Hartkorn (2017)

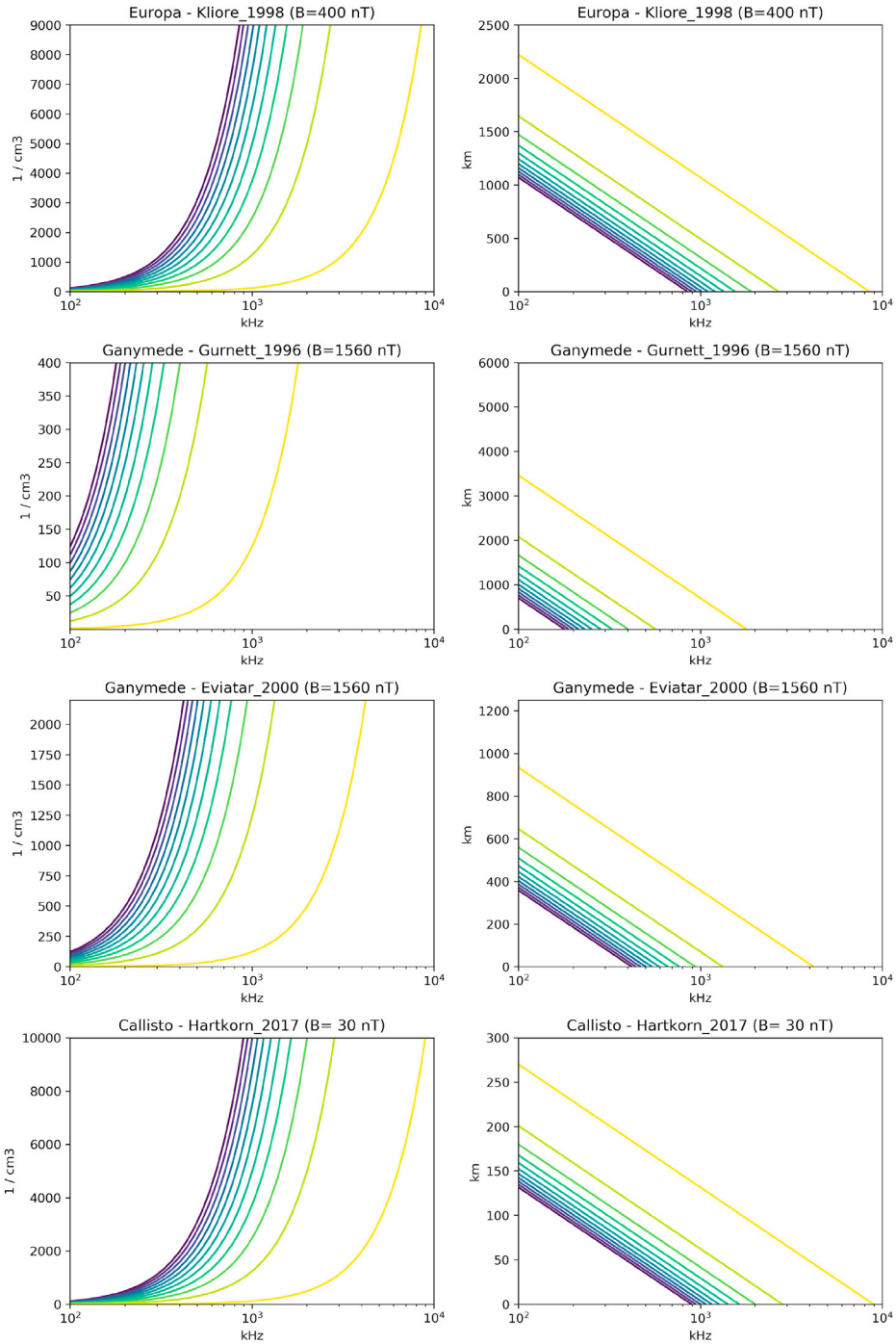

Fig. C.18. Contours of the refractive index values (n^2), for each selected environment models, with 11 contour levels at 0.0, 0.1, 0.2 … 0.9 and 0.99, from left (purple) to right (yellow). From top to bottom: Europa with Kliore (1998), Ganymede with Gurnett et al. (1996) or Eviatar et al. (2001), and Callisto with Hartkorn (2017). The left-hand side columns shows the contour in the plasma density versus frequency space. The right-hand side column shows the altitude versus frequency space.

Table C.7
Estimated parameter thresholds accessible with low frequency radio occultations. The plasma density threshold is a lower limit, while the altitude threshold is an upper limit. Missing values (–) correspond to situations where no refraction is expected, considering no significant refraction occurs for $n^2 > 0.99$.

		Frequency (MHz)					
Quantity	Moon (Reference)	0.7	1	2	5	10	Unit
Plasma Density	*all*	60	125	500	3000	12500	cm^{-3}
Altitude	Europa (Kliore, 1998)	1250	1000	720	270	–	km
Altitude	Ganymede (Gurnett et al., 1996)	1100	700	–	–	–	km
Altitude	Ganymede (Eviatar et al., 2001)	450	360	180	–	–	km
Altitude	Callisto (Hartkorn, 2017)	150	130	90	35	–	km

Appendix D. Supplementary Material Description

The material used to conduct the Galileo flybys' study are provided as a separate data collection (Cecconi et al., 2021, available at https://doi.org/10.25935/8zff-nx36) hosted by PADC (Paris Astronomical Data Centre). For each flyby, the landing page provides access to: (a) the ExPRES products; (b) the Cosmographia context products; (c) a summary dynamic spectrum and (d) the 'pov' movie. The content of (a) and (b) is described below.

Appendix D.1 ExPRES products

The ExPRES data set is composed of four files: (a) an ExPRES configuration file (JSON format), (b) a Galileo spacecraft ephemeris data exported from WebGeoCalc (CSV format), (c) the output ExPRES simulation run data (CDF format), and (d) the observed GLL/PWS data with the superimposed occultation contours (PNG format). Files (a) and (b) contains the ExPRES run parameters and the SPICE Kernels used for the simulation, ensuring the results are reproducible.

Appendix D.2 Cosmographia context products

The Cosmographia data set is composed of a series of subdirectories, organised according to Cosmographia's documentation. It contains all the required configuration catalogue files: the SPICE catalogue file listing the kernels in use for a scene; the spacecraft catalogue file defining the time interval of the scene and the spacecraft reference frame; the modelled radio source catalogue file, derived from an ExPRES simulation run; the ExPRES configuration file and simulation run; and the scripts used to produce the movie output. Two output movies are provided, showing the flyby scenes, as seen from the spacecraft ('pov' labelled movie) and from the top of the Jovian system ('top' labelled movie).

References

Acton, Charles H., 1996. Ancillary data services of NASA's navigation and ancillary information facility. Planet. Space Sci. 44 (1), 65–70. https://doi.org/10.1016/0032-0633(95)00107-7.

Acton, Charles, Bachman, Nathaniel, Semenov, Boris, Wright, Edward, 2018. A look towards the future in the handling of space science mission geometry. Planet. Space Sci. 150, 9–12. https://doi.org/10.1016/j.pss.2017.02.013.

Appleton, E., 1932. Wireless studies of the ionosphere. In: Proceedings of the Wireless Section, Institution of Electrical Engineers, 7, p. 257, 21.

Bruzzone, L., Plaut, J.J., Alberti, G., Blankenship, D.D., Bovolo, F., Campbell, B.A., Ferro, A., Gim, Y., Kofman, W., Komatsu, G., McKinnon, W., Mitri, G., Orosei, R., Patterson, G.W., Plettemeier, D., Seu, R., 2013. RIME: radar for ICY moon exploration. In: 2013 IEEE International Geoscience and Remote Sensing Symposium - IGARSS, pp. 3907–3910. https://doi.org/10.1109/IGARSS.2013.6723686.

Burke, B.F., Franklin, K.L., 1955. Observations of a variable radio source associated with the planet Jupiter. J. Geophys. Res. 60, 213–217. https://doi.org/10.1029/JZ060i002p00213.

Cecconi, Baptiste, 2019. Workflow Studies: Magnetospheres Science and Support to ESA/JUICE Mission Planning. Zenodo. https://doi.org/10.5281/zenodo.2583611.

Cecconi, Baptiste, Zarka, Philippe, 2019. Cassini Rpws Jupiter Encounter Calibrated Dataset v1.0 [dataset]. PADC. https://doi.org/10.25935/H98J-MA66.

Cecconi, B., Hess, S.L.G., Hérique, A., Santovito, Maria Rosaria, Santos-Costa, Daniel, Zarka, Philippe, Alberti, G., Blankenship, D.D., Bougeret, Jean-Louis, Bruzzone, L., Kofman, W., 2012. Natural radio emission of Jupiter as interferences for radar investigations of the icy satellites of Jupiter. Planet. Space Sci. 61, 32–45. https://doi.org/10.1016/j.pss.2011.06.012.

Cecconi, Baptiste, Loh, Alan, Le Sidaner, Pierre, Renaud, Savalle, Bonnin, Xavier, Nguyen, Quynh Nhu, Lion, Sonny, Shih, Albert, Aicardi, Stéphane, Zarka, Philippe, Louis, Corentin, Coffre, Andrée, Lamy, Laurent, Denis, Laurent, Grießmeier, Jean-Mathias, Faden, Jeremy, Piker, Chris, André, Nicolas, Génot, Vincent, Erard, Stéphane, Mafi, Joseph N., King, Todd A., Jim Sky, Demleitner, Markus, 2020. MASER: a science ready toolbox for low frequency radio Astronomy. Data Sci. J. 19 (18), 1062. https://doi.org/10.5334/dsj-2020-012.

Cecconi, Baptiste, Louis, Corentin, Crego, Claudio Muñoz, Vallat, Claire, 2021. Auroral Radio Source Occultation Modeling and Application to the Juice Science Mission Planning. PADC. https://doi.org/10.25935/8ZFF-NX36 supplementary material: Galileo flybys [dataset].

Colin, Lawrence, 1972. Mathematics of Profile Inversion. Technical Report NASA-TM-X-62150. NASA.

Connerney, J.E.P., Acuna, M.H., Ness, N.F., 1981. Modeling the Jovian current sheet and inner magnetosphere. J. Geophys. Res. 86, 8370–8384. https://doi.org/10.1029/JA086iA10p08370.

Connerney, J.E.P., Kotsiaros, S., Oliversen, R.J., Espley, J.R., Joergensen, J.L., Joergensen, P.S., Merayo, J.M.G., Herceg, M., Bloxham, J., Moore, K.M., Bolton, S.J., Levin, S.M., 2018. A new model of Jupiter's magnetic field from Juno's first nine orbits. Geophys. Res. Lett. 45 (6), 2590–2596. https://doi.org/10.1002/2018GL077312.

Connerney, J.E.P., Timmins, S., Herceg, M., Joergensen, J.L., 2020. A jovian magnetodisc model for the Juno era. J. Geophys. Res. Space Phys. 125 (1–11). https://doi.org/10.1029/2020JA028138.

ESA SPICE Service, 2020. JUICE SPICE Kernel Dataset. V2.7 [Dataset]. ESA. https://doi.org/10.5270/esa-ybmj68p.

Eviatar, A., Vasyliunas, V.M., Gurnett, D., 2001. The ionosphere of Ganymede. Planet. Space Sci. 49, 327–336. https://doi.org/10.1016/S0032-0633(00)00154-9.

Gautier, Anne-Lise, Cecconi, Baptiste, Zarka, Philippe, 2013. ARTEMIS-P: a general Ray Tracing code in anisotropic plasma for radioastronomical applications. In: Proceedings of the 2013 International Symposium on Electromagnetic Theory, pp. 1–4.

Grodent, Denis, 2015. A brief review of ultraviolet auroral emissions on giant planets. Space Sci. Rev. 187, 23–50. https://doi.org/10.1007/s11214-014-0052-8.

Gurnett, D.A., Kurth, William S., Shaw, R.R., Roux, A., Gendrin, R., Kennel, C.F., Scarf, F.L., Shawhan, S.D., 1992. The Galileo plasma wave investigation. Space Sci. Rev. 60, 341–355. https://doi.org/10.1007/BF00216861.

Gurnett, D.A., Kurth, W.S., Roux, A., Bolton, S.J., Kennel, C.F., 1996. Evidence for a magnetosphere at Ganymede from plasma-waves observations by the Galileo spacecraft. Nature 384, 535–537. https://doi.org/10.1038/384535a0.

Gurnett, D.A., Kurth, W.S., Granroth, L.J., 1997. GO J PWS REFORMATTED PLAYBACK SPECTRUM ANALYZER FULL V1.0 [Dataset]. *NASA Planetary Data System*. GO-J-PWS-2-REDR-LPW-SA-FULL-V1.0. https://doi.org/10.17189/1519681.

Gurnett, D.A., Kurth, William S., Menietti, J.D., Persoon, A.M., 1998. An unsual rotationally modulated attenuation band in the Jovian hectometric radio emission spectrum. Geophys. Res. Lett. 25 (11), 1841–1844. https://doi.org/10.1029/98GL01400.

Gurnett, D.A., Kurth, W.S., Kirchner, D.L., Hospodarsky, G.B., Averkamp, T.F., Zarka, P., lecacheux, A., Manning, R., Roux, A., Canu, P., Cornilleau-Wehrlin, N., Galopeau, P., Meyer, A., Bostrom, R., Gustafsson, G., Wahlund, J.-E., Åhlen, L., Rucker, H.O., Ladreiter, H.P., Macher, W., Woolliscroft, L.J.C., Alleyne, H., Kaiser, M.L., Desch, M.D., Farrell, W.M., Harvey, C.C., Louarn, P., Kellogg, P.J., Goetz, K., Pedersen, A., 2004. The Cassini radio and plasma wave investigation. Space Sci. Rev. 114 (1–4), 395–463. https://doi.org/10.1007/s11214-004-1434-0.

Harrison, P.A., Rixon, G., 2016. Universal Worker Service Pattern Version 1.1, p. 1024. https://doi.org/10.5479/ADS/bib/2016ivoa.spec.1024H.
Hartkorn, Olivier, 2017. Modeling Callisto's Ionosphere, Airglow and Magnetic Field Environment. Technical Report. Köln Universität.
Hess, S.L.G., Echer, E., Zarka, P., 2012. Solar wind pressure effects on Jupiter decametric radio emissions independent of Io. Planet. Space Sci. 70 (1), 114–125. https://doi.org/10.1016/j.pss.2012.05.011.
Kliore, A.J., 1998. Satellite atmosphere and magnetosphere. In: Highlights of Astronomy, 11B, pp. 1065–1069.
Kumamoto, A., Kasaba, Y., Tsuchiya, F., Misawa, H., Kita, H., Puccio, W., Wahlund, J.E., Bergman, J., Cecconi, B., Goto, Y., Kimura, J., Kobayashi, T., 2017. Feasibility of the exploration of the subsurface structures of Jupiter's icy moons by interference of Jovian hectometric and decametric radiation. In: Fischer, G., Mann, G., Panchenko, M., Zarka, P. (Eds.), Planetary Radio Emissions VIII, pp. 127–136. https://doi.org/10.1553/PRE8s127.
Kurth, William S., Bolton, S.J., Gurnett, D.A., Levin, S., 1997. A Determination of the source of the Jovian hectometric radiation via occultation by Ganymede. Geophys. Res. Lett. 24 (10), 1171–1174. https://doi.org/10.1029/97GL00988.
Lamy, L., Zarka, Philippe, Cecconi, B., Hess, S.L.G., Prangé, Renée, 2008. Modeling of Saturn Kilometric Radiation arcs and equatorial shadow zone. J. Geophys. Res. 113 (A10213). https://doi.org/10.1029/2008JA013464.
Lamy, L., Zarka, P., Cecconi, B., Klein, L., Masson, S., Denis, L., Coffre, A., Viou, C., 2017. 1977-2017: 40 years of decametric observations of Jupiter and the sun with the nancay decameter Array. In: Fischer, G., Mann, G., Panchenko, M., Zarka, P. (Eds.), Planetary Radio Emissions VIII, pp. 455–466. https://doi.org/10.1553/PRE8s455.
Louarn, P., Perraut, S., Roux, A., Gurnett, D.A., Kurth, William S., Bolton, S.J., 1997. Global plasma environment of Io as inferred from the Galileo plasma wave observations. Geophys. Res. Lett. 24, 2115. https://doi.org/10.1029/97GL01850.
Louarn, P., Allegrini, F., McComas, D.J., Valek, P.W., Kurth, W.S., André, N., Bagenal, F., Bolton, S., Connerney, J., Ebert, R.W., Imai, M., Levin, S., Szalay, J.R., Weidner, S., Wilson, R.J., Zink, J.L., 2017. Generation of the jovian hectometric radiation: first lessons from Juno. Geophys. Res. Lett. 44 (10), 4439–4446. https://doi.org/10.1002/2017GL072923.
Louarn, P., Allegrini, F., McComas, D.J., Valek, P.W., Kurth, W.S., André, N., Bagenal, F., Bolton, S., Ebert, R.W., Imai, M., Levin, S., Szalay, J.R., Wilson, R.J., 2018. Observation of electron conics by Juno: implications for radio generation and acceleration processes. Geophys. Res. Lett. 45, 9408–9416. https://doi.org/10.1029/2018GL078973.
Louis, C.K., Hess, S.L.G., Cecconi, B., Zarka, P., Lamy, L., Aicardi, S., Loh, A., 2019a. ExPRES: an exoplanetary and planetary radio emissions simulator. Astron. Astrophys. 627, A30. https://doi.org/10.1051/0004-6361/201935161.
Louis, C.K., Prangé, R., Lamy, L., Zarka, P., Imai, M., Kurth, W.S., Connerney, J.E.P., 2019b. Jovian auroral radio sources detected in situ by Juno/waves: comparisons with model auroral ovals and simultaneous HST FUV images. Geophys. Res. Lett. 46, 11606–11614. https://doi.org/10.1029/2019GL084799.
Louis, Corentin K., Hess, Sébastien L.G., Cecconi, Baptiste, Zarka, Philippe, Lamy, Laurent, Aicardi, Stéphane, Loh, Alan, 2020. Maserlib/Expres: Version 1.1.0. Zenodo. https://doi.org/10.5281/zenodo.4292002 [software].
Marques, M.S., Zarka, P., Echer, E., Ryabov, V.B., Alves, M.V., Denis, L., Coffre, A., 2017. Statistical analysis of 26 yr of observations of decametric radio emissions from Jupiter. Astron. Astrophys. 604, A17. https://doi.org/10.1051/0004-6361/201630025.
Menietti, J.D., Gurnett, D.A., Hospodarsky, G.B., Higgins, C.A., Kurth, William S., Zarka, Philippe, 2003. Modeling radio emission attenuation lanes observed by the Galileo and Cassini spacecraft. Planet. Space Sci. 51, 533–540. https://doi.org/10.1016/S0032-0633(03)00078-3.
Modolo, R., Hess, S., Génot, V., Leclercq, L., Leblanc, F., Chaufray, J.Y., Weill, P., Gangloff, M., Fedorov, A., Budnik, E., Bouchemit, M., Steckiewicz, M., André, N., Beigbeder, L., Popescu, D., Toniutti, J.P., Al-Ubaidi, T., Khodachenko, M., Brain, D., Curry, S., Jakosky, B., Holmström, M., 2018. The LatHyS database for planetary plasma environment investigations: overview and a case study of data/model comparisons. Planet. Space Sci. 150, 13–21. https://doi.org/10.1016/j.pss.2017.02.015.
Morioka, A., Miyoshi, Y., Tsuchiya, F., Misawa, H., Kasaba, Y., Asozu, T., Okano, S., Kadokura, A., Sato, N., Miyaoka, H., Yumoto, K., Parks, G.K., Honary, F., Trotignon, Jean-Gabriel, Décréau, Pierrette, Reinisch, B.W., 2011. On the simultaneity of substorm onset between two hemispheres. J. Geophys. Res. Space Phys. 116 (15), A04211. https://doi.org/10.1029/2010JA016174.
Piker, C., Granroth, L., Mukherjee, J., Pisa, D., Cecconi, B., Kopf, A., Faden, J., 2019. Lightweight federated data networks with das2 tools. Earth Space Sci. Open Archive. https://doi.org/10.1002/essoar.10500359.1.
Romero-Wolf, Andrew, Vance, Steve, Frank, Maiwald, Heggy, Essam, Ries, Paul, Liewer, Kurt, 2015. A passive probe for subsurface oceans and liquid water in Jupiter's icy moons. Icarus 248, 463–477. https://doi.org/10.1016/j.icarus.2014.10.043.
Schroeder, Dustin M., Romero-Wolf, Andrew, Carrer, Leonardo, Grima, Cyril, Campbell, Bruce A., Kofman, Wlodek, Bruzzone, Lorenzo, Blankenship, Donald D., 2016. Assessing the potential for passive radio sounding of Europa and Ganymede with RIME and REASON. Planet. Space Sci. 134 (C), 52–60. https://doi.org/10.1016/j.pss.2016.10.007.
Servillat, Mathieu, Riebe, Kristin, Boisson, Catherine, Bonnarel, François, Galkin, Anastasia, Louys, Mireille, Nullmeier, Markus, Renault-Tinacci, Nicolas, Sanguillon, Michèle, Ole Streicher, 2020. IVOA Provenance Data Model Version 1.0. page 411.
Servillat, Mathieu, Aicardi, Stéphane, Cecconi, Baptiste, Mancini, Marco, 2021a. OPUS: an Interoperable Job Control System Based on VO Standards. *arXiv e-prints*, art. arXiv:2101.08683.
Servillat, Mathieu, Bonnarel, François, Louys, Mireille, Sanguillon, Michèle, 2021b. Practical Provenance in Astronomy. *arXiv e-prints*, art. arXiv:2101.08691.
Wahlund, J.E., 2013. The radio & plasma wave investigation (RPWI) for JUICE. In: EPSC. EPSC2013–637.
Witasse, Olivier, 2019. JUICE (Jupiter Icy Moon Explorer): a European mission to explore the emergence of habitable worlds around gas giants. In: EPSC-DPS Joint Meeting 2019. EPSC-DPS. EPSC–DPS2019–400.
Zarka, P., 2004. Radio and plasma waves at the outer planets. Adv. Space Res. 33 (11), 2045–2060. https://doi.org/10.1016/j.asr.2003.07.055.
Zarka, Philippe, Cecconi, B., Kurth, William S., 2004. Jupiter's low-frequency radio spectrum from Cassini/Radio and Plasma Wave Science (RPWS) absolute flux density measurements. J. Geophys. Res. 109, A09S15. https://doi.org/10.1029/2003JA010260.